Effects of Series Resistance and Inductance on Solar Cell Admittance Measurements[a]

John H. Scofield[b]

Department of Physics, Oberlin College, Oberlin, OH 44074

Admittance measurements have been performed on a variety of 0.43 cm^2 area, copper indium gallium diselenide (CIGS) polycrystalline thin film solar cells for frequencies (f) ranging from 1 kHz to 1 MHz and bias voltages (V) ranging from -2.0 to 0.2 V. The bulk of these measurements are not presented here. To extend the usefulness of these measurements, and in particular, to extract information about traps, it is first necessary to account for frequency-dependent effects associated with the series resistance and inductance. Such is the purpose of this paper. The complex admittance of a four-element circuit is calculated and compared with measurements on two typical CIGS solar cells. The model circuit consists of a capacitance C in parallel with a resistance r, with this combination in series with a resistor R and inductor L. C accounts for the depletion capacitance of the diode, and R and r account for series and shunt resistances typically observed in solar cell current-voltage measurements. The series inductance was introduced to account for observed resonance effects in the admittance measurements. Model calculations are shown to be in good agreement with measurements on devices. For our cells, measurements above 300 kHz are seldom useful, as these frequencies are in the regime where series R and L dominate the behavior of the circuit. We find measurements in the 10 -50 kHz range to be most appropriate for determining charge densities from C-V scans.

1. Introduction

The frequency- and voltage-dependencies of the complex admittance of a reverse biased PN junction can yield useful information about the junction. The capacitance (C) of a well-behaved reverse-biased diode, for instance, gives an indirect measure of the depletion width. For an ideal, uniformly doped, one-sided junction, a plot of $1/C^2$ versus bias voltage is expected to yield a straight line whose slope may be used to determine the lesser of the two doping densities [1]. For non-uniform doping, the doping density as a function of distance from the junction (determined by the depletion width) may be obtained from the derivative, $d(1/C^2)/dV$, where V is the bias voltage [2].

The AC capacitance measures the mobile charge density within a small distance δW (determined by the AC voltage δV) at the edge of the depletion width W (determined by the DC bias voltage V). Trapped charge can respond to low frequencies but not to high frequencies, where high and low are determined by the relaxation time of the trap. Thus, traps contribute to the low-frequency capacitance, but not to the high-frequency capacitance [3,4,5]. In principle, trap distributions may be extracted from measurements of capacitance versus frequency.

Finally, measurements of the diode conductance may be used also be used to identify traps [6]. Equilibrium (i.e., zero bias) measurements for a range of frequencies and temperatures have been used to extract trap densities and energy levels [6, 7].

While the frequency-dependence of the junction capacitance may, in principle, be used to identify trapping states and their time constants, series resistance and inductance introduce additional frequency dependence, complicating the analysis. Here the admittance is calculated for a model circuit consisting of a capacitance (C) in parallel with a shunt resistance (r), with these in series with a second resistance (R) and an inductance (L). For reasonable quality cells it is assumed that r >> R. It is shown that for frequencies well below $1/(2\pi rC)$, the real and imaginary parts of the admittance approach $1/r$ and $2\pi fC$ respectively. Behavior at higher frequencies is determined by the other time constant, RC, and the resonant frequency, $(2\pi(LC)^{1/2})^{-1}$. Various cases are discussed.

The calculations are compared with measurements from 13-16% efficient, 0.43 cm^2 copper indium gallium

---

diselenide solar cells. Measurements are found to be qualitatively in agreement with calculations, with noticeable differences thought to be associated with trapping effects. Measurements for the frequency range 1-100 kHz are found to be most useful for theses cells. Measurements above 300 kHz were seldom useful due to the effects of series resistance and inductance. Thus, commercial C-V systems that operate at a single frequency of 1 MHz, designed for use with crystalline materials, are not useful for studying the capacitance of these solar cells, and are unlikely to be useful for polycrystalline solar cells generally.

Measurements were performed in the dark with cells usually in reverse bias which is not, of course, the useful regime for solar cell operation. Nevertheless, such admittance measurements yield information about carrier and trap densities relevant to solar cell operation.

2. Circuit Model

2.1 Complex Admittance

The voltage and frequency dependencies of a diode in reverse bias can give useful information about doping densities and densities of extraneous states near the junction. Most capacitance meters, or the more general impedance meters, model the impedance of the diode as a capacitor (C) and resistor (r) in parallel. What is measured is the complex admittance of this circuit, $\mathbf{A}$, given by

$$A(\mathbf{w}) \equiv \frac{1}{Z(\mathbf{w})} = G_m(\mathbf{w}) + jwC_m(\mathbf{w}), \quad (1)$$

where $j \equiv \sqrt{-1}$, $\mathbf{Z}$ is the complex impedance, $\omega \equiv 2\pi f$ is the angular frequency, C_m is the measured capacitance and G_m is the measured conductance. It is useful to note that the measured conductance and capacitance are given by

$$G_m(\mathbf{w}) \equiv \mathrm{Re}\{A(\mathbf{w})\} \quad (2)$$
$$C_m(\mathbf{w}) \equiv \mathbf{w}^{-1} \mathrm{Im}\{A(\mathbf{w})\}.$$

For the above circuit, the simple relationship that $G_m = 1/r$ and $C_m = C$ is obtained. In the absence of extraneous states both G_m and C_m will be independent of frequency. For the National Renewable Energy Laboratory (NREL) CIS and CIGS test cells having area = 0.43 cm^2, at zero bias capacitance and shunt resistances range from 8 to 20 nF and 0.5 to 500 kΩ respectively. Note that C scales with cell area while both r and R scale inversely with cell area. While it is common practice to express these quantities in units of F/cm^2 and Ω cm^2 respectively, in this paper capacitance, resistance, inductance, and conductance will be expressed in the MKS units of farads (F), ohms (Ω), henries (H), and siemens (S) respectively.

2.2 Equivalent Circuit for Thin Film Solar Cell

In practice, polycrystalline thin film solar cells also have series resistance (R) which needs to be included in the model. The series resistance may be associated with the contacts, or it may be internal to the diode itself. Moreover,

the measurement circuit must introduce some series inductance. Thus modified, the measurement circuit appears in Figure 1. The self-inductance of a wire segment is on the order of 0.5 µH per foot [8]. For NREL CIS and CIGS test solar cells, series resistances have a range R = 0.2 to 20 Ω.
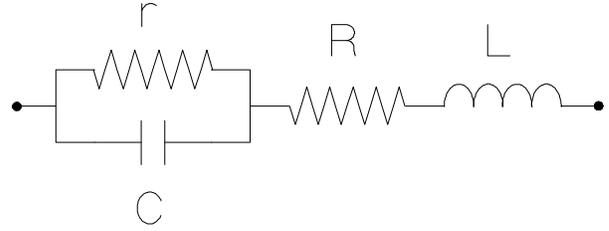
FIG. 1. More realistic circuit model for a solar cell in reverse bias including series resistance and inductance.

The complex impedance of the circuit shown in Figure 1 is given by

$$Z(\mathbf{w}) = R + jwL + \frac{r \cdot (jwC)^{-1}}{r + (jwC)^{-1}}. \quad (3)$$

As before, the measured capacitance and conductance are related to the real and imaginary parts of the admittance. Inverting the above equation and solving for the real and imaginary parts one finds

$$G_m(\mathbf{w}) = \frac{1}{r} \frac{1 + \dfrac{R}{r} + w^2 rRC^2}{\left(1 + \dfrac{R}{r} - w^2 LC\right)^2 + w^2 \left(RC + \dfrac{L}{r}\right)^2} \quad (4)$$

$$C_m(\mathbf{w}) = C \frac{1 - \dfrac{L/r}{rC} - w^2 LC}{\left(1 + \dfrac{R}{r} - w^2 LC\right)^2 + w^2 \left(RC + \dfrac{L}{r}\right)^2}. \quad (5)$$

Before discussing the frequency dependence of the above equations it is useful to define three characteristic times for the problem. These are:

$$\begin{aligned} t_1 &\equiv rC, \\ t_2 &\equiv RC, \\ t_L &\equiv L/r. \end{aligned} \quad (6)$$

The indexing of the two R-C time constants is chosen to reflect the ordering of their characteristic frequencies. For any reasonable solar cell, the series resistance will be much smaller than the shunt resistance, and accordingly, the ordering of the characteristic frequencies will be $f_1 \ll f_2$, f_L, where

$$2pf_1 \equiv w_1 \equiv t_1^{-1},$$
$$2pf_2 \equiv w_2 \equiv t_2^{-1}, \qquad (7)$$
$$2pf_L \equiv w_L \equiv t_L^{-1}.$$

It is also useful to express the ratio r/R by

$$l^2 \equiv R/r. \qquad (8)$$

Later equations will be simplified by considering the case where $\lambda^2 \ll 1$. In terms of the three time constants and the resistance ratio, the expressions above may be rewritten as

$$G_m(w) = \frac{1}{r} \frac{1 + l^2 + w^2 t_1 t_2}{\left(1 + l^2 - w^2 t_1 t_L\right)^2 + w^2 \left(t_2 + t_L\right)^2}, \qquad (9)$$

$$C_m(w) = C \frac{1 - \dfrac{t_L}{t_1} - w^2 t_1 t_L}{\left(1 + l^2 - w^2 t_1 t_L\right)^2 + w^2 \left(t_2 + t_L\right)^2}. \qquad (10)$$

It is also useful to look at the phase $\Theta_m(\omega) \equiv \mathrm{Arg}\{A(\omega)\} = \tan^{-1}\{\omega C_m/G_m\}$, given by

$$\Theta_m(w) = \tan^{-1}\left\{ \frac{w\left[t_1 - t_L\left(1 + w^2 t_1^2\right)\right]}{1 + l^2 + w^2 t_1 t_2} \right\}. \qquad (11)$$

Finally, note that the product $\tau_1 \tau_L$ is related to the L-C resonant frequency f_0 by

$$t_1 t_L = LC \equiv t_0^2 \equiv w_0^{-2} \equiv (2pf_0)^{-2}. \qquad (12)$$

3. Frequency Dependence for Model Circuit

3.1 Zero Inductance

As the frequency-dependence described by the above equations is generally complicated, the initial discussion of these equations is restricted to the case where L = 0. In this limit, the equations reduce to

$$G_m(w) = \frac{1}{r} \frac{1 + l^2 + w^2 t_1 t_2}{\left(1 + l^2\right)^2 + w^2 t_2^2} = \begin{cases} \dfrac{1}{r}\dfrac{1}{1 + l^2}, & w \to 0 \\ \dfrac{1}{R}, & w \to \infty \end{cases}, \qquad (13)$$

and

$$C_m(w) = \frac{C}{\left(1 + l^2\right)^2 + w^2 t_2^2} = C \begin{cases} \dfrac{1}{\left(1 + l^2\right)^2}, & w \to 0 \\ \dfrac{1}{w^2 t_2^2}, & w \to \infty \end{cases}. \qquad (14)$$

For the case of $\lambda^2 \ll 1$, these expressions simplify to

$$G_m(w) = \begin{cases} \dfrac{1}{r} & w \to 0 \\ \dfrac{1}{R}, & w \to \infty \end{cases}, \qquad (15)$$

and

$$C_m(w) = C \begin{cases} 1, & w \to 0 \\ 1/(w^2 t_2^2), & w \to \infty \end{cases}. \qquad (16)$$

These equations are graphed in Figure 2 for realistic values of C, r, and R.
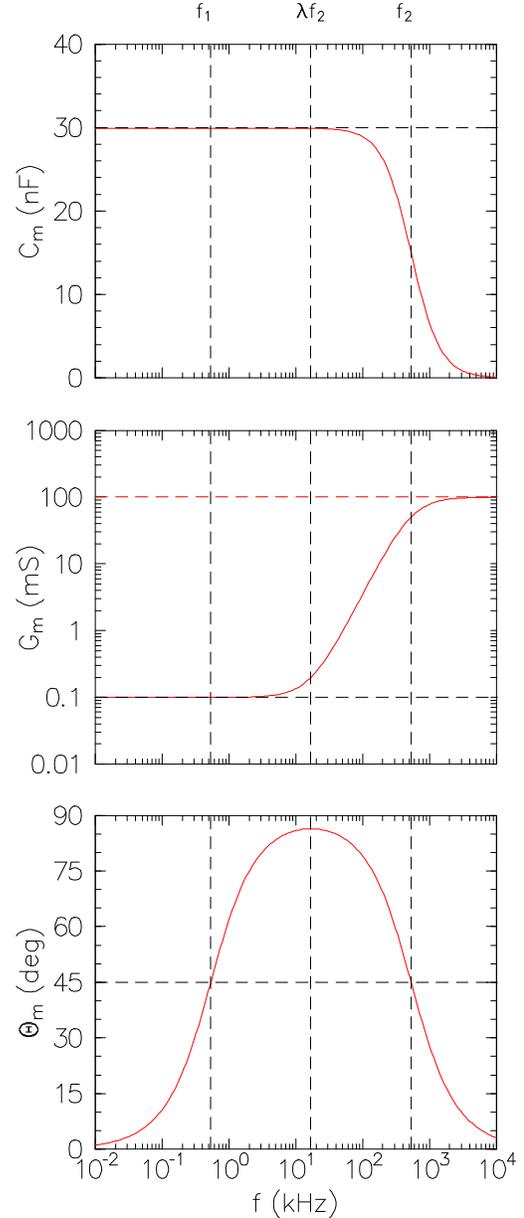
FIG. 2. Calculated frequency dependence of a) the measured capacitance, b) measured conductance, and c) the phase angle for the model circuit for L = 0, C = 30 nF, r = 10 kΩ, and R = 10 Ω. The vertical dashed lines correspond to the frequencies $f_1 (\approx 530$ Hz), $\lambda f_2 = (f_1 f_2)^{1/2}$, and $f_2 (\approx 530$ kHz). The horizontal dashed lines

correspond to a) the circuit capacitance C, b) 1/r and 1/R, and c) 45 degrees.

The three frequencies f_1, $\lambda f_2 = (f_1 f_2)^{1/2}$, and f_2 divide the frequency domain into four distinct regions. In the low-frequency regime ($f \ll f_1$) $C_m = C$ and $G_m = 1/r$. For high frequencies ($f \gg f_2$) $C_m = 0$ and $G_m = 1/R$. Most of the transition in the capacitance and conductance occurs in the range $\lambda f_2 < f < f_2$. Not much occurs in the lower of the two intermediate regimes, $f_1 < f < \lambda f_2$, where C_m remains constant and G_m changes by a factor of two. Note that $\Theta_m = 45°$ at frequencies where $f = f_1$ and $f = f_2$, and has a maximum value near 90° for $f = (f_1 f_2)^{1/2}$. The calculations show that C_m deviates from C at high frequencies, but that $C_m = C$ for arbitrarily low frequencies. In practice, however, it has been observed that capacitance measurements become unreliable whenever $\Theta_m < 20°$ [5].

3.2 Non-zero Inductance

Consider the high- and low-frequency limits of the admittance for non-zero inductance; these are

$$G_m(w) = \frac{1}{r} \begin{cases} \dfrac{1}{1+l^2}, & w \to 0 \\ \dfrac{l^2}{w^2 t_L^2}, & w \to \infty \end{cases} \qquad (17)$$

and

$$C_m(w) = C \begin{cases} \dfrac{1 - t_L/t_1}{(1+l^2)^2}, & w \to 0 \\ \dfrac{-1}{w^2 t_1 t_L}, & w \to \infty \end{cases} . \qquad (18)$$

The low-frequency conductance is unchanged by the introduction of series inductance as expected. The high-frequency conductance, and both the low- and high-frequency capacitances are changed, however. For the 0.43 cm^2 cells used in our study, $\tau_L/\tau_1 \ll 1$, so that series inductance has negligible effects on the low-frequency capacitance. This need not be the case for larger area cells as τ_L/τ_1 is proportional to cell area. as the cell capacitance scales with the cell area and the shunt resistance scales inversely with the area.

At sufficiently high frequencies, inductive effects are substantial, as the measured capacitance changes sign. Of course the capacitance is not negative, the problem is that the circuit has become inductive and it no longer makes sense to interpret the imaginary part of the admittance as ωC_m.

Physically, the introduction of inductance has lead to a resonance, with resonant frequency $2\pi f_0 = \omega_0 = (\tau_1 \tau_L)^{-1/2} = (LC)^{-1/2}$. The circuit behavior depends on where the resonant frequency lies relative to the previously mentioned characteristic frequencies, $f_1 = \lambda^2 f_2$, λf_2, and f_2. Since the inductance is generally small, the resonant frequency will

typically be quite high. Therefore, only the two cases 1) $f_2 < f_0$ and 2) $f_2 > f_0$ need be considered.

3.2.1 Case $f_2 < f_0$

For experiments, the few feet of wire in the measurement circuit suggests that a few μH is an appropriate estimate for L. The curves in Figure 3 are calculated with the same parameters as were those in Figure 2, except that L = 0.5 μH.

In the above figures note that at the resonant frequency f_0, the measured capacitance goes negative, the measured conductance peaks, and the phase angle is equal to zero.

3.2.2 Case $f_2 > f_0$

This situation occurs for larger inductance and/or lower series resistance. This situation is illustrated in Figure 4, where curves were generated with L = 10 μH and other parameters as before.
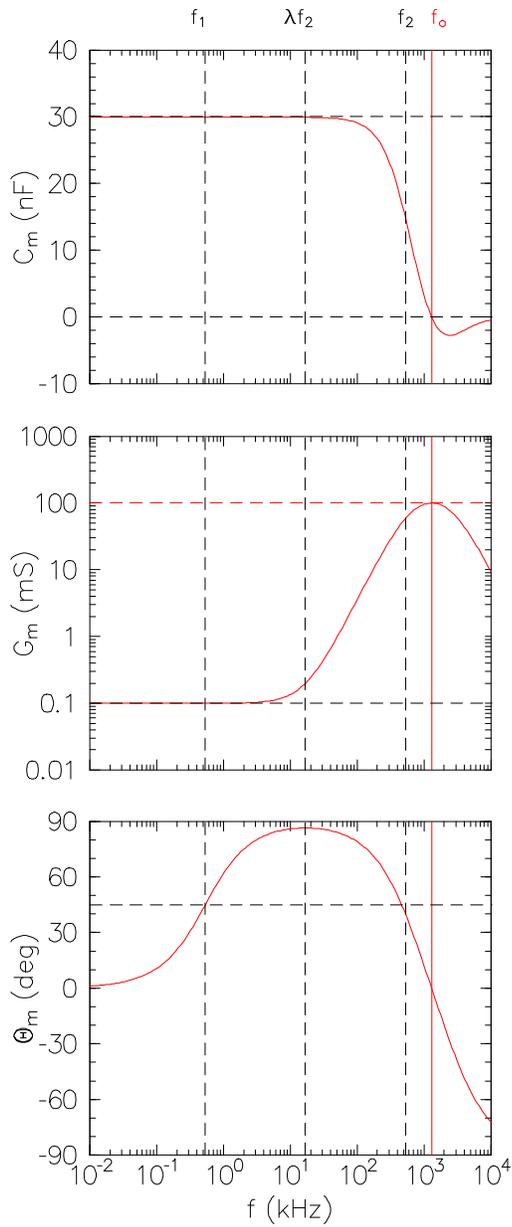
FIG. 3. Calculated frequency dependence of a) the measured capacitance, b) measured conductance, and c) the phase angle for the model circuit for $L = 0.5$ μH, $C = 30$ nF, $r = 10$ kΩ, and $R = 10$ Ω. The vertical dashed lines correspond to the frequencies f_1, $\lambda f_2 = (f_1 f_2)^{1/2}$, f_2, and the resonant frequency $f_o \approx 1.3$ MHz. The horizontal dashed lines correspond to a) zero and the circuit capacitance C, b) 1/r and 1/R, and c) 45 degrees.
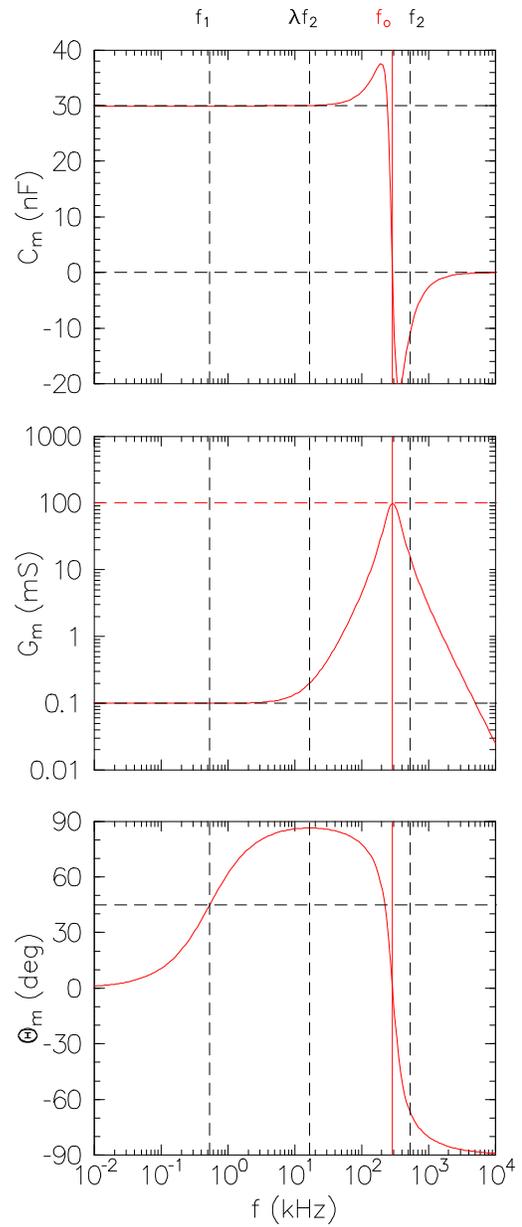
FIG. 4. Calculated frequency dependence of a) the measured capacitance, b) measured conductance, and c) the phase angle for the model circuit for $L = 10$ μH, $C = 30$ nF, $r = 10$ kΩ, and $R = 10$ Ω. The vertical dashed lines correspond to the frequencies $f_1 (\approx 530$ Hz), $\lambda f_2 = (f_1 f_2)^{1/2}$, and f_2 (≈ 530 kHz). The vertical solid line corresponds to the resonant frequency $f_o \approx 290$ kHz. The horizontal dashed lines correspond to a) zero and the circuit capacitance C, b) 1/r and 1/R, and c) 45 degrees.

4. Comparison with Measurements for a Test Circuit

To test the validity of the above calculations and the reliability of the measurement apparatus, the circuit of Figure 1 was constructed from two resistors and a capacitor. Series inductance was not deliberately introduced, but arose from the residual self-inductance of the connecting cables.

Measurements were performed for frequencies ranging from 100 Hz to 10 MHz. Circuit elements were chosen to be C = (10.0 ± 0.2) nF, r = (1000 ± 20) Ω, and R = (2.0 ± 0.2) Ω. The circuit elements were wired inside a small metal box with separate current and voltage leads brought to four grounded BNC connectors mounted on the box. Four-probe and two-probe admittance measurements were performed using an HP model 4192A LRC meter connected to the circuit.

Four-probe measurements were performed with four, 36" long BNC cables connected to the separate voltage- and current- jacks of the HP LRC meter. The results of these measurements are shown in Figure 5. Solid squares are measurements while the curves represent calculations for parameter values of C = (9.6 ± 0.2) nF, r = (1000 ± 50) Ω, R = (3.0 ± 0.2) Ω, and L = (80 ± 10) nH.[1] The separate voltage and current probes minimize the effects of the cable series resistance and inductance. For this case the resonant frequency f_0 is just slightly higher than f_1. The discrepancy between the actual value of R and that which, when entered into the model calculations, causes them to agree best with the measurements, is not understood. Neither is the origin of the
observed frequency dependence for C_m at low frequencies understood.

We also performed two-probe admittance measurements for this circuit, as these best mimic the measurements performed on solar cells. Two-probe measurements result in additional series resistance and inductance associated with the connecting cables. Measurements were performed using the same leads as those used for subsequent measurements on solar cells, except that two additional 12 in. clip leads were used complete the connections. The results of these measurements are shown in Figure 6. As before, the solid squares represent measurements while the curves represent the calculations, in this case for C = (9.8 ± 0.2) nF, r = (1000 ± 50) Ω, R = (4.4 ± 0.2) Ω, and L = (2.7 ± 0.1) μH. The main difference between these two-probe and the previously-discussed four-probe measurements is the significantly larger series inductance. The 2.7 μH inductance is reasonable for the nearly 6 ft. long leads that connect the circuit to the LRC meter. The two-probe measurements also suffer from an additonal 1.2 Ω series resistance.

5. Comparison with Measurements on CIGS Solar Cells

The above serves to outline the complicated frequency-dependent capacitance and conductance that result from measurements on solar cells due simply to series resistance

---

[1] Values of C, L, R, and r were chosen so as to yield the best agreement with the data as determined by visual inspection. Here, the "uncertainties" represent the amount by which the particular parameter could be varied before the agreement between calculations and data was noticeably worse.

and inductance. In all cases, the low-frequency capacitance is a good measure of C. For cells with low series resistance the tendency is to observe a frequency dependent capacitance, conductance, and phase angle similar to that shown in Figure 3. For cells having high series resistance the data tends to be more like that shown in Figure 4.
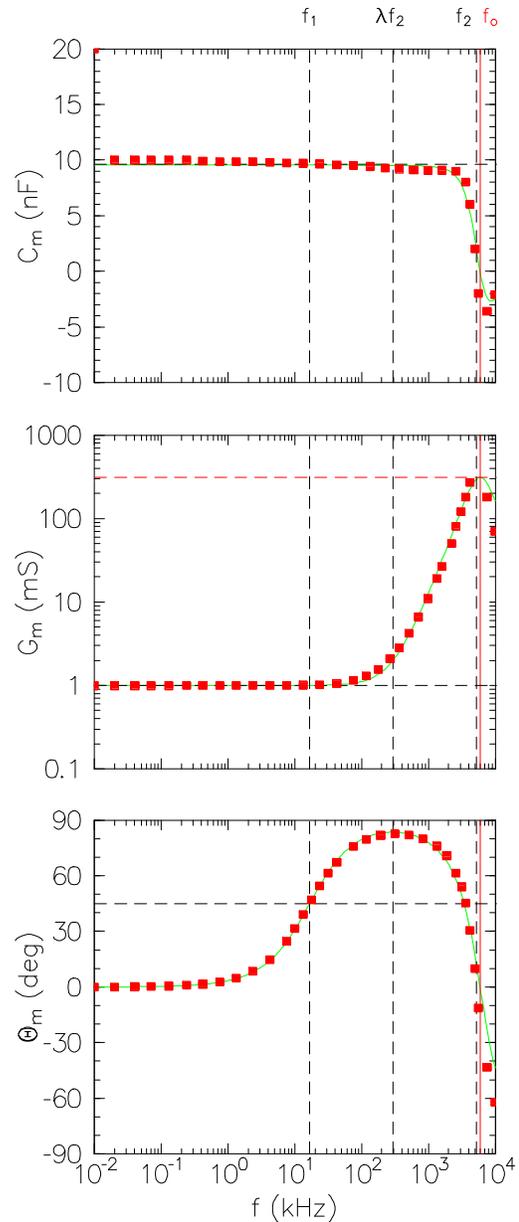
FIG. 5. Measured (symbols) and calculated (curves) a) capacitance, b) conductance, and c) phase angle for two resistors and a capacitor wired as shown in Figure 1. The component values were C = 10.0 nF, r = 1.0 kΩ, and R = 2.0 Ω. The curves were calculated using C = (9.6 ± 0.2) nF, r = (1000 ± 50) Ω, R = (3.0 ± 0.2) Ω, and L = (80 ± 10) nH. The measurements were performed with separate current and voltage connections, minimizing the series contribution of the connecting cables.

In Figure 7, calculations are compared with zero-bias admittance data for NREL CIGS solar cell C253-23-9. The

properties of this cell under illumination are shown in Table I. Listed are the cell efficiency (η), short circuit current density (J_{SC}), open circuit voltage (V_{OC}), and fill factor (FF). For this cell, the resonance frequency $f_0 < f_1$, leading to an up-turn in C(f) at high frequencies similar to that exhibited in Figure 4 above. The solid curves in Figure 7 represent model calculations for C = 11.2 nF, r = 350 kΩ, R = 5 Ω, and L = 1.6 µH. The characteristic frequencies for these parameters are f_1 = 41 Hz, f_2 = 2.84 MHz, f_0 = 1.19 MHz, and the resistance ratio is $\lambda^2 = 1.43 \times 10^{-5}$.

same two-probe arrangement that was used for subsequent measurements on solar cells, increasing the series contribution (both L and R) of the connecting cables.

Figure 7(a) shows that the low-frequency capacitance is not exactly constant, but instead, increases slightly at lower frequencies indicating the presence of some traps. The importance of traps is even more noticeable in Figure 7(b) in the same frequency range, where the measured and calculated conductances deviate even more significantly.

FIG. 6. Measured (symbols) and calculated (curves) a) capacitance, b) conductance, and c) phase angle for two resistors and a capacitor wired as shown in Figure 1. The component values were C = 10.0 nF, r = 1.0 kΩ, and R = 2.0 Ω. The curves were calculated using C = (9.8 ± 0.2) nF, r = (1000 ± 50) Ω, R = (4.4 ± 0.2) Ω, and L = (2.7 ± 0.1) µH. The measurements were performed with the
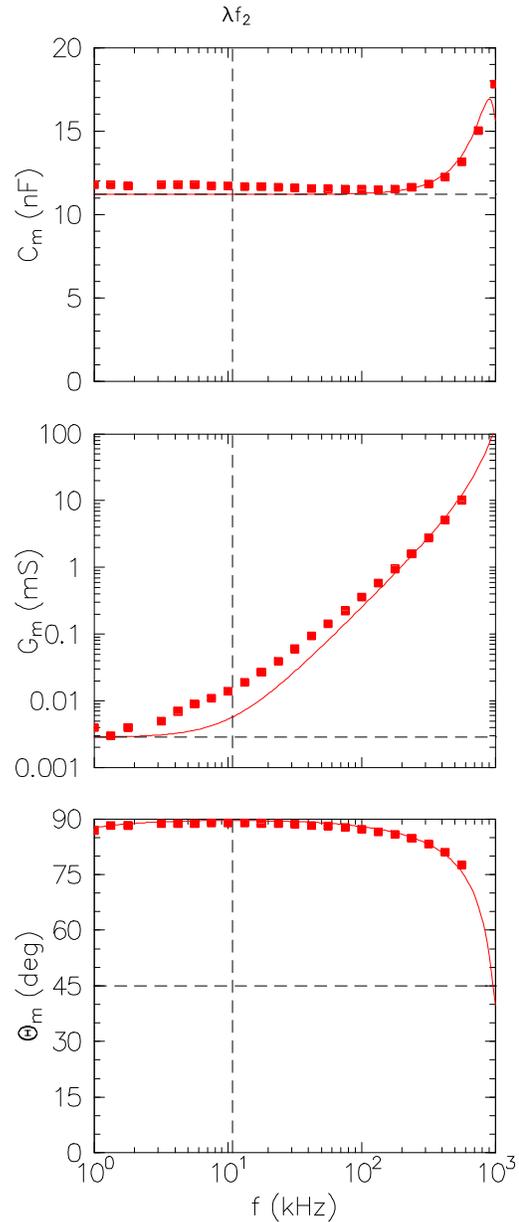
FIG. 7. Graphs of the frequency dependence of a) the measured capacitance, b) measured conductance, and c) the phase angle for L = 1.6 µH, C = 11.2 nF, r = 350 kΩ, and R = 5.0 Ω. Solid curves are calculated while solid squares are data from device C253-23-9 with V = 0.

Admittance data from a second cell, C257-12-7, are compared with calculations in Figure 8. The *solid squares*

represents equilibrium measurements (V = 0) while the *open triangles* are measurements for a bias V = -2.00 V.[2] Due to the higher series resistance of this cell, the resonance frequency $f_0 > f_1$, leading to a frequency-dependent capacitance similar to that shown in Figure 3.
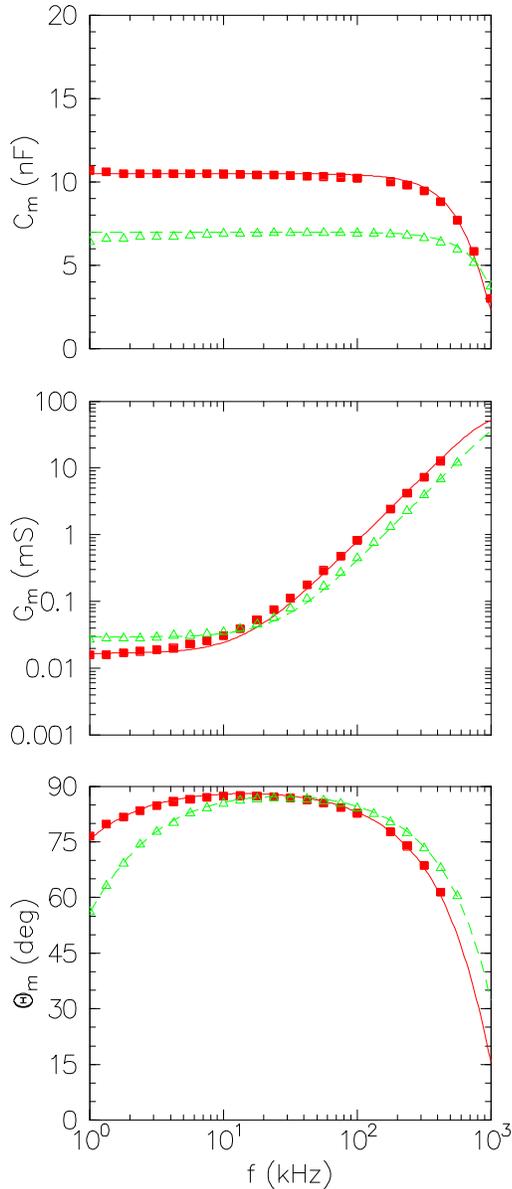
FIG. 8. Graphs of the frequency dependence of a) the measured capacitance, b) measured conductance, and c) the phase angle for cell C257-12-7. The solid squares were measured with V = 0 while the open triangles were measured with V = -2.00 V. The solid and dashed lines represent model calculations.

The solid curves are model calculations for C = 10.5 nF, r = 60 kΩ, R = 18 Ω, and L = 1.6 μH. The characteristic frequencies for these parameters are f_1 = 250 Hz, f_2 =

842 kHz, f_0 = 3.1 MHz, and the resistance ratio is $\lambda^2 = 3.00 \times 10^{-4}$. The dashed curves are model calculations for C = 7.0 nF, r = 34 kΩ, R = 20 Ω, and L = 1.6 μH. The characteristic frequencies for these parameters are f_1 = 669 Hz, f_2 = 1.14 MHz, f_0 = 3.7 MHz, and the resistance ratio is $\lambda^2 = 5.880 \times 10^{-4}$. As compared with the previous cell, Figure 8(a) and (b) show that the low-frequency capacitance is nearly constant and the low-frequency conductance hardly deviates from the expected curve, indicating the relative unimportance of traps in this sample. [3]

The reverse-bias conductance data of Figure 8(b) agree better with the model calculation than do the zero-bias data for the same cell. This is because of the wider depletion width, and the fact that more traps tend to be located close to the junction than farther away. In all of our measurements we find the effects of trapping to be decreased for more negative bias. Also note that both C and r vary with V. The voltage-dependence of C is, of course, fully expected, and is the basis for C-V measurements. This voltage-dependent shunt resistance is observed for all of the polycrystalline devices investigated. For some cells the shunt resistance is found to decrease by more than an order of magnitude as V varies from 0 to -2.0 V. This effect, due to some type of breakdown phenomenon, will not be further explored here.

Finally, it is important to note that the values of r and R extracted from these measurements do not always agree with those determined from current-voltage curves. For the shunt resistance, this is not surprising since the admittance measurements yield a value of r for each bias voltage while, for J-V measurements, a single value of r is extracted from measurements for different voltages -- *assuming* that r is constant. The greater series resistances extracted from admittance measurements may simply be due to the fact that these measurements were performed with common current and voltage probes (i.e., 2-probe) while the J-V measurements were performed with separate current and voltage probes (i.e., 4-probe). 4-probe measurements are less susceptible to contact resistance contributions than are 2-probe measurements. It is unlikely, however, that the 18 Ω series resistance required to model the observed admittance measurements for device C257-12-7 can thus be explained

---

[2] Negative voltages correspond to reverse bias while positive voltages correspond to forward bias.

[3] The reverse-bias capacitance decreases slightly at lower frequencies. This is an artifact associated with transient effects in the cell combined with the method in which data are recorded. The cell is initially held in equilibrium for a few minutes, then the bias voltage is rapidly switched to -2.0 V. During the next 5 seconds the actual voltage across the cell rapidly decays to about -1.85 V. V continues to decay slowly during the next three minutes or so while the excitation frequency is swept from 1 kHz to 1 MHz and the admittance data are recorded. At the end of the sweep, V has a typical value of -1.75 V. Thus, during the period of the sweep, the depletion capacitance increases slightly

6. Implications for C-V Measurements

These calculations have implications for the usual C-V measurements used to extract free carrier densities. First, it is obvious that one should choose a measurement frequency f so that it is well below both f_2 and f_0. This is best determined by performing measurements of $C_m(f)$ versus frequency for several voltages spanning the range of biases to be used for the subsequent C-V measurements. Note that f_2 and f_0 both vary with voltage, shifting to higher frequencies as the V is made more negative (i.e., wider depletion width). Thus, if one determines a satisfactory f at the greatest bias voltage to be used (i.e., narrowest depletion width), this same f will remain well below f_2 and f_0 as the bias voltage is decreased (i.e., wider depletion width). The voltage may be swept in either direction, but it is very important to be sure that $f \ll f_2, f_0$ at the greatest bias voltage. This is particularly problematic if measurements are to be performed into forward bias. Whatever the choice of f, as $V \rightarrow V_{bi}$ (from below) the depletion width approaches zero and f_2, f_0 will ultimately shift below f. Again, it is safer to choose a satisfactory f at the greatest bias voltage to be used and to sweep voltages negative from there.

From the above perspective one would want to choose the lowest measurement frequency possible. The lower the measurement frequency, however, the more that traps contribute to the measured capacitance, and the more error introduced into the deduced free charge carrier density. To minimize the effects of traps one wishes to use a higher measurement frequency. Combining this criteria with our earlier discussion it seems that a measurement frequency

$$\mathbf{f} = \sqrt{\mathbf{f_1 f_2}} = \mathit{l}\,\mathbf{f_2} \text{ is an appropriate choice.}$$

These ideas are illustrated by C-V measurements on device C257-12-7, shown in Figure 9. The 1 MHz data deviate from measurements for lower frequencies for most of the range of bias voltage. The 500 kHz data are in agreement with lower frequency measurements for V < -0.5 V, but deviate for higher voltages. The 300 kHz data show hints of deviation at the very highest bias voltage. Doping profiles for this range of voltages determined from the slopes of the curves for f < 300 kHz are all in agreement.
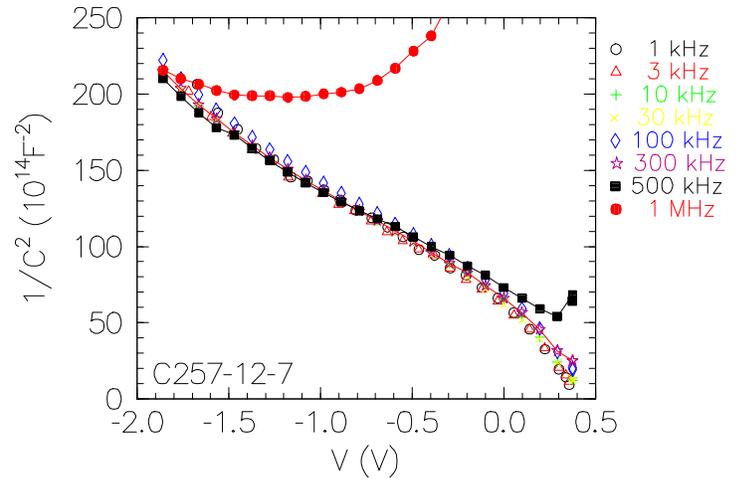
FIG. 9. Plots of $1/C^2$ versus bias voltage for various measurement frequencies. All measurements are in agreement for -1.8 V bias, but the 1MHz data deviate from the rest for V > -1.7 V, and the 500 kHz data deviate for V > -0.5 V.

6. Summary and Conclusions

The frequency-dependence of the admittance of polycrystalline CIGS solar cells in reverse bias has been measured and compared with the calculations for a simple circuit. At low frequencies the admittance is found to be that of the depletion capacitance (C) in parallel with a shunt resistance (r). At higher frequencies the measurements are strongly affected by series resistance (R) and inductance (L). Depending on the relative values of the characteristic frequencies $f_1 = 1/(2\pi RC)$ and $f_0 = \{2\pi(LC)^{1/2}\}^{-1}$, the "measured" capacitance is found to either decrease ($f_1 < f_0$) or increase at high frequencies. For all of the 0.43 cm^2 area, CIGS cells investigated, reliable C-V measurements were obtained only with f < 300 kHz, with f = 50 kHz being the recommended measurement frequency.

Acknowledgments

(a) This work was supported, in part, by an AWU-DOE faculty sabbatical fellowship.

(b) Present address: National Renewable Energy Laboratory, 1617 Cole Blvd., Golden, CO 80401

[1] See, for instance, S. M. Sze, *Physics of Semiconductor Devices, 2nd edition.* (John Wiley & Sons, New York, 1981).

[2] L. C. Kimerling, *J. Appl. Phys.* **45** (4), 1839-45 (1974).
     "Influence of deep traps on the measurement of free-carrier
     distributions in semiconductors by junction capacitance
     techniques."

[3] E. Schibli and A. G. Milnes, *Solid-State Electron.* **11**, 323-
     334 (1968). "Effects of deep impurities on n^+p junction
     reverse-biased small-signal capacitance."

[4] H. Tavakolian and J. R. Sites, in *Proc. 18th IEEE
     Photovoltaic Specialists Conf.,* 1065-68 (Oct. 1985).
     "Capacitance determination of interfacial states in $CuInSe_2$
     solar cells."

[5] Peter H. Mauk, Hossein Tavakolian, and James R. Sites,
     IEEE Trans. Electron Devices **ED-37** (2), 422-427 (1990).
     "Interpretation of thin-film polycrystalline solar cell
     capacitance."

[6] D. L. Losse, *J. Appl. Phys.* **46** (5) 2204-14 (1975).
     "Admittance spectroscopy of impurity levels in Schottky
     barriers."

[7] L. B. Fabick and K. L. Eskenas, in *Proc. of the 18th IEEE
     PVSC,* Oct. 21-25, 1985, Las Vegas, pp. 754-757.
     "Admittance spectroscopy and application to $CuInSe_2$
     photovoltaic devices."

[8] See, for instance, Ralph Morrison, *Grounding and Shielding
     Techniques in Instrumentation* (Wiley, New York, 1986), p.
     153.